A&A 396, 473–487 (2002)
DOI: 10.1051/0004-6361:20021426

Astronomy & Astrophysics

Tidal dwarfs in the M81 group: The second generation?⋆,⋆⋆

L. N. Makarova[1,2], E. K. Grebel[3], I. D. Karachentsev[1], A. E. Dolphin[4], V. E. Karachentseva[5], M. E. Sharina[1,2], D. Geisler[6], P. Guhathakurta[7,8], P. W. Hodge[9], A. Sarajedini[10], and P. Seitzer[11]

[1] Special Astrophysical Observatory of the Russian Academy of Sciences, Nizhnij Arkhyz 369167, Karachaevo-Cherkessia, Russia
e-mail: lidia@sao.ru, ikar@luna.sao.ru
[2] Isaac Newton Institute of Chile, SAO Branch, Russia
[3] Max-Planck Institute for Astronomy, Königstuhl 17, 69117 Heidelberg, Germany
[4] Kitt Peak National Observatory, National Optical Astronomy Observatories, PO Box 26732, Tucson, AZ, 85726, USA
[5] Astronomical Observatory of Kiev University, 04053, Observatorna 3, Kiev, Ukraine
[6] Departamento de Fisica, Grupo de Astronomia, Universidad de Concepción, Casilla 160-C, Concepción, Chile
[7] Herzberg Fellow, Herzberg Institute of Astrophysics, 5071 W. Saanich Road, Victoria, B.C. V9E 2E7, Canada
[8] Permanent address: UCO/Lick Observatory, University of California at Santa Cruz, Santa Cruz, CA 95064, USA
[9] Department of Astronomy, University of Washington, PO Box 351580, Seattle, WA 98195, USA
[10] Department of Astronomy, University of Florida, Gainesville, FL 32611, USA
[11] Department of Astronomy, University of Michigan, 830 Dennison Building, Ann Arbor, MI 48109, USA

Received 25 July 2002 / Accepted 24 September 2002

Abstract. We derive quantitative star formation histories of the four suspected tidal dwarf galaxies in the M 81 group, Holmberg IX, BK3N, Arp-loop (A0952+69), and Garland, using Hubble Space Telescope/Wide Field Planetary Camera 2 images in F606W and F814W obtained as part of a Snapshot survey of dwarf galaxies in the Local Universe. We consider the spatial distribution and ages of resolved stellar populations in these dwarf irregular galaxies. We use synthetic color-magnitude diagrams to derive the ages of the major star formation episodes, star formation rates, and approximate metallicity ranges. All the galaxies show evidence of continuous star formation between about 20 and 200 Myr ago with star formation rates in the range 7.5×10^{-3}–7.6×10^{-4} $M_{\odot}$ yr^{-1}. The metallicity of the detected stars spans a wide range, and have lower than solar abundance. A possible scenario is that all four dwarf galaxies were formed from material in the metal-poor outer part of the giant spiral galaxy M 81 after the tidal interaction between M 81, M 82, and NGC 3077 ~ 200 Myr ago. While we do not directly detect pronounced old stellar populations, the photometric limits of our data are such that the presence of such a population is not entirely ruled out.

Key words. galaxies: dwarf – galaxies: photometry – galaxies: stellar content – galaxies: interactions – galaxies: individual: M 81 – galaxies: evolution

1. Introduction

Galaxy interactions are still common at the present epoch and can have a significant impact on the appearance and evolution of galaxy groups and clusters. The closest examples of ongoing interactions can be found in our immediate surroundings: The Milky Way is currently accreting the Sagittarius dwarf spheroidal (dSph) galaxy (Ibata et al. 1994) and interacts with the Magellanic Clouds (e.g., Gardiner et al. 1994). Evidence for more dramatic interactions involving an entire galaxy group can be seen in the nearby M 81 group, whose dominant members M 81, M 82, NGC 3077, and NGC 2976 are embedded in a huge H I cloud with extended tidal H I bridges between the components (van der Hulst 1977; Appleton et al. 1981; Yun et al. 1994). Past surveys for dwarf galaxies in the M 81 group led to the identification of a large number of dwarf galaxy candidates (Börngen & Karachentseva 1982; Karachentseva et al. 1985; van Driel et al. 1998; Boyce et al. 2001; Karachentsev et al. 2001). Some of the concentrations visible in the H I bridges have candidate optical counterparts identified as dwarf galaxies. It has been suggested that some of these dwarf galaxies are tidally disrupted dwarfs (e.g., Karachentseva et al. 1985),

Send offprint requests to: L. N. Makarova, e-mail: lidia@sao.ru

⋆ Based on observations with the NASA/ESA Hubble Space Telescope, obtained at the Space Telescope Science Institute, which is operated by the Association of Universities for Research in Astronomy, Inc., under NASA contract NAS 5-26555. These observations are associated with proposal ID GO-8192.

⋆⋆ Table 1 is only available in electronic form at the CDS via anonymous ftp to cdsarc.u-strasbg (130.79.128.5) or via http://cdsweb.u-strasbg.fr/cgi-bin/qcat?J/A+A/396/473

while others may be dwarfs newly formed in the tidal tails (e.g., van Driel et al. 1998).

Owing to its proximity (mean distance 3.7 Mpc; Karachentsev et al. 2002) the M81 group offers a unique opportunity to study the properties of tidal dwarf galaxy candidates in great detail. Of particular interest are the evolutionary histories of the potential tidal dwarfs and the effect of tidal interaction on star formation.

In the framework of our Hubble Space Telescope (HST) snapshot survey of nearby dwarf galaxy candidates (programs SNAP 8192 and 8601, PI: Seitzer) we have imaged 25 galaxies in the M 81 group (Karachentsev et al. 1999, 2000, 2001, 2002). Photometric distances of these galaxies were obtained using the tip of red giant branch (TRGB), a well-established distance indicator (e.g., Lee et al. 1993).

Here we present an analysis of data on four dwarf irregular galaxies located in the tidal H I features of the M 81 group (Holmberg IX, BK3N, Arp-loop and Garland). In Sect. 2 we describe the observations, reduction and photometric errors analysis. In Sect. 3 we discuss the resulting color-magnitude diagrams. In Sect. 4 a quantitative analysis of star formation in the galaxies is given. Section 5 contains a general discussion of star formation history and evolution of the galaxies, as well as the conclusions.

2. Observations and data reduction

The galaxies were observed with the Hubble Space Telescope during 2000 July 30–2001 June 27 with the Wide Field and Planetary Camera (WFPC2) as a part of the Dwarf Galaxy Snapshot Survey (Seitzer et al. 1999; Grebel et al. 2000). For each target, two exposures of 600 s each were obtained, one in the F606W filter and one in the F814W filter.

Stellar photometry of the galaxies was carried out by A. E. Dolphin with the HSTphot program (Dolphin 2000a). Before running photometry, the data quality images were used to mask bad pixels (*mask* procedure of the HSTphot package). Bright cosmic rays were then masked out using the HSTphot *cleansep* utility. The stellar photometry was obtained simultaneously on the F606W and F814W frames with the *multiphot* procedure. HSTphot uses a library of model PSFs based on Tiny Tim. Changes of the focus of HST were corrected using the residuals of bright, isolated stars. Resulting instrumental magnitudes of $0\farcs5$ radius were corrected for charge-transfer inefficiency and calibrated using the relations of Dolphin (2000b). We estimate the uncertainty of the photometric zeropoint to be within $0\fm05$ (Dolphin 2000b). Only stars of better photometric quality were used for further analysis. We selected stars with photometric errors less than 0.2 mag, $\chi \leq 2$, and $-0.3 \leq$ sharpness ≤ 0.3 in both filters. Photometry results for the galaxies are presented in Table 1, which is available only in electronic form at the CDS[1]. This table contains 1650 stars measured in the Holmberg IX field, about 300 stars in the BK3N field, about 3200 stars in the Garland field and about 250 stars in the Arp-loop field.

[1] Via anonymous ftp to `cdsarc.u-strasbg` (130.79.128.5) or via `http://cdsweb.u-strasbg.fr/cgi-bin/qcat?J/A+A/396/473`

Data processing and photometric reduction procedures were identical to the ones used in our previous studies of nearby dwarf galaxy candidates (see, for example, Dolphin et al. 2001).

Artificial star tests were performed for each of the galaxies using the same reduction procedures. These tests allow us to estimate the accuracy and completeness of our photometry (see Fig. 1). As was noted earlier (Dolphin et al. 2001), the ~90% maximum completeness level is primarily a result of the fraction of stars falling within one pixel of a masked pixel (cosmic ray, bad pixel, bad column, etc.) and are thus rejected.

3. Color-magnitude diagrams

3.1. Distance and reddening

Color–magnitude ($V - I$, I) diagrams of the four galaxies under consideration are presented in Fig. 2. Galactic extinction is not large for these galaxies: $A_I = 0\fm15$ for Holmberg IX, $A_I = 0\fm16$ for BK3N and Arp-loop and $A_I = 0\fm13$ for Garland, according to Schlegel et al. (1998). The Galactic extinction correction was not made in Fig. 2 in order to facilitate the comparison with the M 81 CMD below (Fig. 3), which also was not corrected for Galactic extinction. Isochrones of appropriate metallicities and ages from Girardi et al. (2000) are shown in the color-magnitude diagrams (CMDs). The isochrones were shifted by the appropriate Galactic extinction and the galaxies' distance moduli. The M 81 Cepheid distance modulus ($\mu_0 = 27.80$ mag, Freedman et al. 1994) was taken for the three galaxies Holmberg IX, BK3N, and Arp-loop. For Garland we used the distance modulus obtained from the tip of the red giant branch (TRGB) of the NGC 3077 halo population (Karachentsev et al. 2002). BK3N and Arp-loop also have TRGB distance estimations (which agree within errors with the Cepheid distance, see Karachentsev et al. (2002)), but whether the detected red giants belong to the galaxies is unclear. We also cannot suggest a significantly larger distance for the objects since they are clearly detected in the core M 81 H I complex. The metallicity specified in each diagram is the metallicity of the theoretical isochrones shown according to our best-fit models. We did not estimate a metallicity from the color and slope of the red giant branch stars, because these stars are too close to the photometric detection limit.

The color-magnitude diagrams in Fig. 2 are quite typical for dwarf irregular galaxies. We can see the upper main sequence and probable helium-burning blue loop stars, the red supergiant branch and probably also some young and intermediate age AGB stars for all of the galaxies. There are no clear signs of an RGB in the Holmberg IX CMD, as was already noted by Karachentsev et al. (2002). The apparent absence of an old stellar population may be direct evidence of the recent formation of Holmberg IX (see next section for details). In contrast to Holmberg IX, Garland shows a clump of stars at faint magnitudes that consists very likely of RGB stars. These, however, may belong to the nearby NGC 3077 galaxy, not to Garland itself (see also Sakai & Madore 2001). The other two irregular dwarfs show a slightly increased number of stars at $I > 24$ mag,

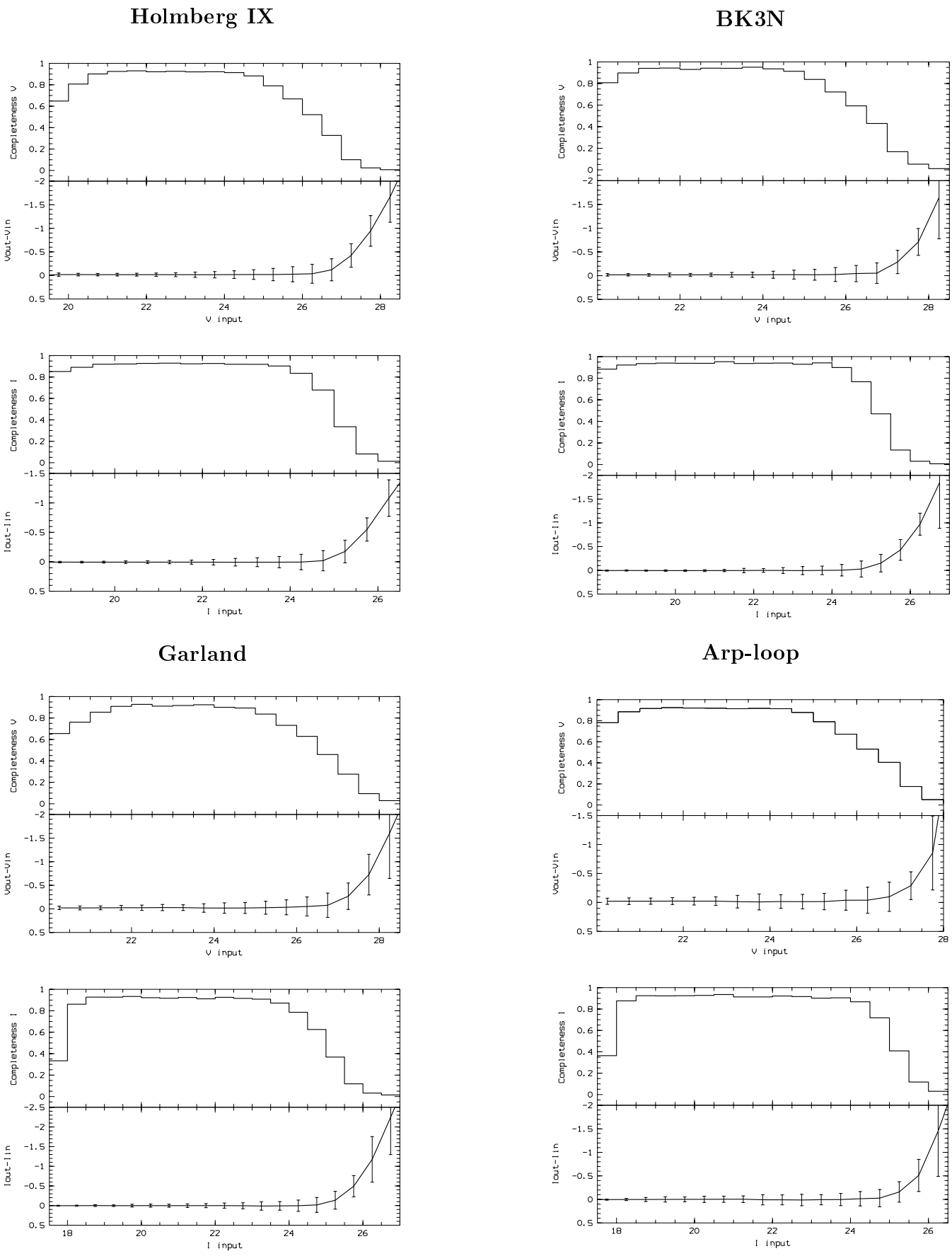

Fig. 1. *V* and *I* completeness (upper panel) and photometric errors (bottom panel) for the dwarf galaxies. In the bottom panel for each galaxy error bars show the 1σ distribution.

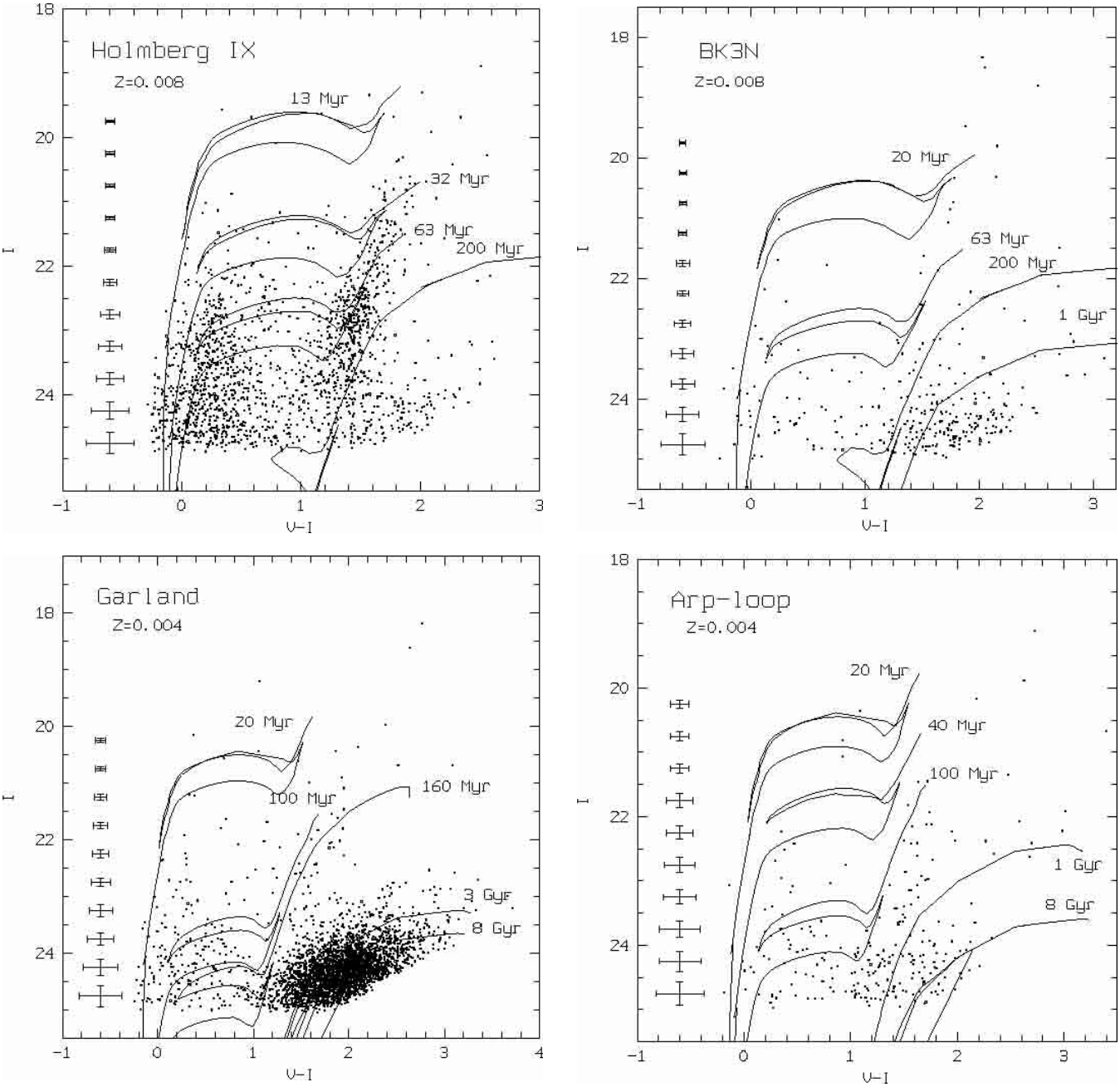

Fig. 2. I, $V-I$ color-magnitude diagrams of the dwarf irregular galaxies. The error bars on the left side of each panel show 1 σ distribution of the photometric errors. Isochrones by Girardi et al. (2000) are overplotted in the CMDs.

which may be indicative of the tip of their respective red giant branches.

3.2. Foreground/background contamination

As we can see from Fig. 2, the color-magnitude diagrams of the suspected tidal dwarfs are not heavily contaminated by foreground stars. The expected number of Galactic foreground stars in the magnitude range $18\overset{m}{.}0 \leq I \leq 20\overset{m}{.}0$ would be roughly two or three in the WFPC2 field according to the star counts of Bahcall & Soneira (1981). We have made also independent number counts of the stars in the CMDs of 24 observed dwarf galaxies of the M 81 group in the same magnitude range $18\overset{m}{.}0 \leq I_0 \leq 20\overset{m}{.}0$ and in the color range $1.4 \leq (V-I)_0 \leq 3.0$. We included data for M 81 group dwarf irregulars as well as dwarf spheroidals in these counts. (NGC 2366 was excluded, because it contains 22 bright stars in this area.) The mean number of stars fulfilling these selection criteria is 2.4 with a standard deviation of 2.4. Confining ourselves to the nine dwarf spheroidals in the M 81 group for which we have HST data, we find stellar number counts of 1.2 ± 1.5 in the afore described range. These numbers are in good agreement with the Bahcall & Soneira (1981) model. Number counts for fainter magnitudes may be significantly contaminated by red supergiant branch stars of the irregular galaxies. The number of stars in the magnitude range $18\overset{m}{.}0 \leq I \leq 22\overset{m}{.}0$ and in the

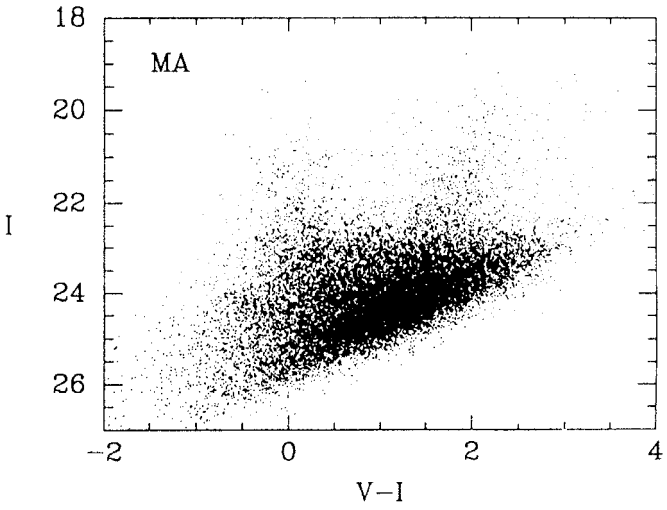

Fig. 3. CM diagram of M 81 major axis field from Hughes et al. (1994). Reproduced by permission of the AAS.

color range $1.4 \leq (V-I)_0 \leq 3.0$ for dwarf spheroidal galaxies is 3.4 ± 2. Therefore, we expect between 1 to 5 foreground stars in the magnitude range $18\overset{m}{.}0 \leq I \leq 22\overset{m}{.}0$ and in the color range $1.4 \leq (V-I)_0 \leq 3.0$ in WFPC2 field.

The color-magnitude diagrams of Holmberg IX, BK3N, and Arp-loop may also be contaminated by stars belonging to the close spiral galaxy M 81. For comparison we show a $V-I, I$ CMD of M 81 in Fig. 3. This diagram was taken from Hughes at al. (1994). It shows a field along M 81's major axis at an angular distance from the nucleus of about 5′.5. The observations were made with the Wide Field Camera (WFC) aboard the Hubble Space Telescope as a part of the Extragalactic Distance Scale Key Project. The color-magnitude diagram in Fig. 3 was not corrected for Galactic extinction. We can see upper main sequence stars, red supergiant branch (RSGB) stars, and red giant branch stars in this diagram. The blue plume and RSGB are very wide. The RGB falls in the region of large photometric errors. As was noted by Hughes at al. (1994), the color spread observed in M 81 is probably due to a combination of photometric errors and variable reddening across the field. The red supergiant population seems also to be very red in general. Based on H II region observations, the mean abundance of recently formed stars is 12+log(O/H) = 8.85 (i.e., about the solar abundance) for this field (Freedman et al. 1994). Note that Galactic extinction is nearly the same for M 81 and for the three dwarf irregulars. The color-magnitude diagram of M 81 is $\sim 1\overset{m}{.}5$ deeper in I than our CMDs and it contains ten times more stars. As can be seen from the comparison of the CMDs in Figs. 2 and 3, the relatively well-populated RSGB of Holmberg IX has slightly bluer colors than the majority of M 81's red supergiants. The red supergiant branch of Holmberg IX is also considerably more narrow than in M 81, which appears to indicate low internal extinction (in addition to a possibly lower metallicity). The poorly populated RSGBs of BK3N and Arp-loop generally agree with the location of Holmberg IX's RSGB in the CMDs. Also, the blue features in the diagrams of the dwarfs and in M 81's CMD have the same overall location. The red giant branch of M 81 in Fig. 3 appears to extend farther to redder colors by at least ~0.5 mag than observed in our dwarfs, which may indicate that a number of red giants in M 81 have a higher metallicity than the few red giants in the dwarf galaxies. On the other hand, we cannot exclude reddening effects introduced by variable extinction intrinsic to M 81, and effects of photometric errors on this close to the photometric limit area of the CMD. Also, we can not exclude contamination of our CMDs by M 81 red giants, if M 81 has an extended old halo population.

All of our data may be contaminated by background galaxies and quasars. While the excellent resolution of HST's WFPC2 allows us to reject many galaxies based on their extended light profiles, a few quasars may contribute to the point-source number counts at blue colors.

4. Star formation history of the tidal dwarfs

It is well known that the central galaxies of the M 81 group are strongly interacting. There is a huge cloud of intergalactic H I encompassing M 81, M 82, NGC 3077 and NGC 2976 (Appleton et al. 1981; Yun et al. 1994). The image of the hydrogen complex from the paper of Yun et al. (1994) is shown in Fig. 4. This strong interaction may be a reason for the formation of tidal dwarf galaxies from a condensed interstellar medium that was stripped from the main body of one of the galaxies in the interacting system.

Recently results of a blind H I survey of the M 81 group were published by Boyce et al. (2001). It was suggested in this article that Holmberg IX and Arp-loop may have recently condensed from the tidal debris between M 81 and M 82 (see Fig. 4). The origin of Garland is uncertain, although it is plausibly associated with the tidal interaction of NGC 3077 with M 81 (Karachentsev et al. 1985). Recently Heithausen & Walter (2000) revealed a giant molecular cloud in the Garland region with a mass of about $3 \times 10^7\ M_\odot$. Van Driel et al. (1998) suggested that Garland may be at an intermediate stage in the conversion of a tidal tail into a dwarf galaxy. It was noted by Boyce et al. (2001), that the origin of BK3N is rather controversial. The object may be a tidal dwarf galaxy, condensing from the tidal debris of the spur. Alternatively, BK3N may be a pre-existing dIrr galaxy undergoing an interaction with M 81.

Below we attempt to make a quantitative measurement of the star formation history of Holmberg IX, BK3N, Garland and Arp-loop. We consider the spatial distribution and ages of the resolved stellar populations in these possible tidal dwarfs in some detail and try to elucidate the origin of these galaxies.

4.1. The method

We used the starFISH package by Harris & Zaritsky (2001) for the star formation history analysis. This package is intended to determine the best-fit star formation history (SFH) of a mixed stellar population. The package constructs a library of synthetic CMDs based on theoretical isochrones, and determinations of the interstellar extinction, photometric errors, and distance modulus based on the observational data. These synthetic CMDs are combined linearly and compared to the observed CMDs using χ^2 statistics. We used theoretical

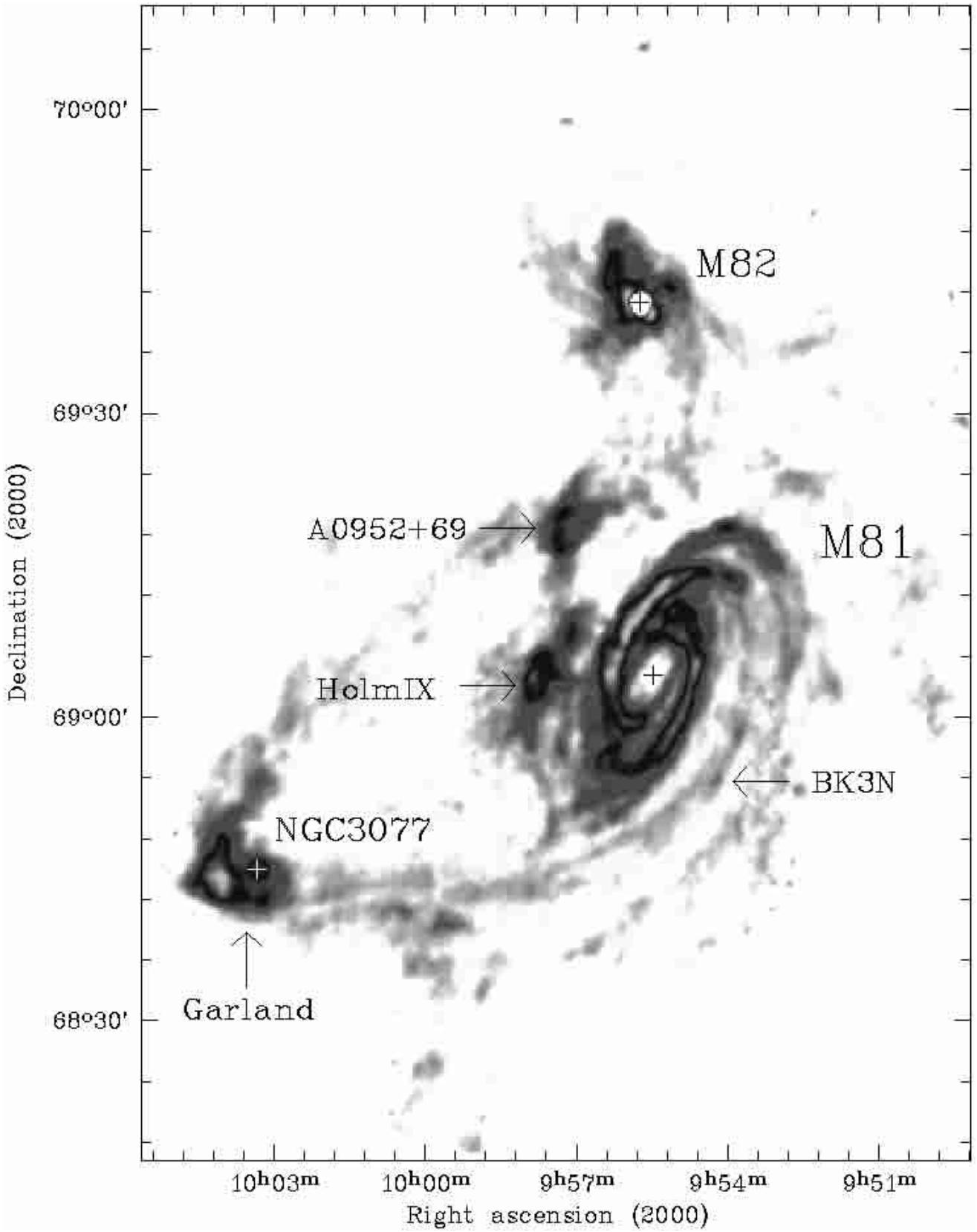

Fig. 4. Integrated HI map of the core M 81 group from Yun et al. (1994). Reproduced by permission of the Nature.

isochrones from the Padua group (Girardi et al. 2000). To include also isochrones with $Z = 0.001$ and log(Age) < 7.8 we complemented this set by earlier work of the same group for these ages and metallicity (Bertelli et al. 1994). Merging these sets did not affect our calculations, because the isochrones of the neighboring metallicities $Z = 0.0004$ and $Z = 0.004$ show

considerable differences only for stars with masses greater than 40 $M_\odot$. Such massive stars are not present in our data.

Each isochrone gives us absolute magnitudes and color indices (including Johnson-Cousins V and I) of a stellar population with a particular age and metallicity. The program transforms these magnitudes into a synthetic CMD by accounting for the following input parameters: galaxy distance, interstellar extinction, initial mass function (IMF), binary fraction, and photometric errors. We constructed the CMDs from isochrones of the full available age range (from $10^{6.6}$ yr to $10^{10.2}$ yr) with a step of log(Age) = 0.2. We are not aware of any metallicity estimations from other studies of Holmberg IX, BK3N, and Arp-loop. The metallicity of red giant stars in the halo of NGC 3077 near the Garland region was estimated photometrically by Sakai & Madore (2001) from their HST/WFPC2 CMD to be $Z = 0.005$. Therefore, for all the galaxies a number of fits were made with different metallicity combinations using the entire range of the available metallicities from $Z = 0.0004$ to $Z = 0.019$. The best solutions were then chosen taking into account χ^2–goodness-of-fit parameter and also the general agreement between the observed CMD and the synthetic CMD constructed from the star formation history (SFH) solution. We have no information about internal extinction in the dwarf galaxies. Therefore, some experiments with differential extinction values for young and old stars were made. The introduction of additional internal extinction for young stars, which mainly populate the CMDs, gave us an RSGB that was too wide and scattered and also some additional scatter in the blue features. As a result, only Galactic extinction was used for the calculation. Detailed photometric errors and completeness data from our artificial star tests were also inserted. We used the default values for the IMF (the Salpeter law) and the binary fraction equal to 0.5. Each resulting model CMD represents a stellar population with the age and metallicity of the parent isochrone. A linear combination of these CMDs forms a composite model CMD that can represent any SFH. The amplitude associated with each CMD is proportional to the number of stars formed at that age and metallicity. The best-fit SFH is described by the set of amplitudes that produces the composite model CMD most similar to the observed CMD. The best-fitting amplitudes are determined by using a modified downhill simplex algorithm (see Harris & Zaritsky 2001).

Our photometry of the stars in the dwarf galaxies contains only stars sufficiently luminous to be detectable in 10-min exposures with HST/WFPC2. The number of stars in the CMDs is low (about 250 in Arp-loop, for example). These factors make the calculations especially difficult, and uncertainties in the SFR estimation are rather large (see below). Nevertheless, most of the galaxies have goodness-of-fit $\chi^2 < 10$. These are quite good results according to J. Harris (starFISH User's Guide).

4.2. Holmberg IX

There are no clear signs of the red giant branch in the CMD of this object, as was already noted by Karachentsev et al. (2002) (see Fig. 2). The resolved stellar populations are mainly blue and red supergiant stars. These two branches are relatively well populated, which distinguishes Holmberg IX from the other three galaxies. The spatial distribution of the various populations in Holmberg IX is shown in Fig. 5. The stars in the area $(V-I)_0 \geq 0.8$ mag and $23\overset{\mathrm{m}}{.}75 \leq I_0 \leq 24\overset{\mathrm{m}}{.}5$ are distributed rather homogeneously across the field. They do not show any concentration towards the galaxy body and may be old red giants belonging to M 81. Upper main sequence stars (MS) are concentrated clearly in the visible star formation areas of the galaxy. The blue loop and red supergiants show a clear increase in density toward the central regions of Holmberg IX. Only the upper, luminous part of the blue population ($I_0 \leq 23\overset{\mathrm{m}}{.}75$) is shown in Fig. 5. When all the blue stars in Holmberg IX's CMD ($I_0 \leq 24\overset{\mathrm{m}}{.}5$) are plotted instead, the central concentration becomes less pronounced, indicating that recent star formation was indeed strongly centrally concentrated. For a general discussion of population gradients in dwarf galaxies, see Harbeck et al. (2001). A full mapping of the more extended, fainter/older populations requires a larger field of view than the partial coverage of Holmberg IX afforded by our HST/WFPC2 pointing.

The best-fit SFH for Holmberg IX is shown in Fig. 6. For this model the χ^2 value is 8.1. The model CMD constructed from this SFH is shown at the right panel of Fig. 7. For comparison the original CMD of the galaxy is displayed in the left panel of Fig. 7. As can be seen from the comparison of these two panels, there are differences between the diagrams. The observed groups of red and blue stars are generally slightly redder (about 0.1–0.2 mag in $V-I$). The differences between observed and model data are most clear in the RSGB slope, which is somewhat steeper for the model branch. Introducing additional extinction does not improve the solution. The red supergiant branch is sensitive especially to this internal extinction, which produces too much scatter as compared to the observed RSGB. The model CMD in Fig. 7 contains fewer bright blue and red supergiants. This lack is common for the model CMDs of all four dwarfs. The very small number of the brightest stars in the original data makes statistical analysis and modelling especially difficult in this part of the diagram. This may be the main reason for the deficiency of the brightest stars in the model diagram relative to this population of the original data. A number of red giants, which probably belong to M 81, are also reproduced in Fig. 7. Their age was estimated to be about 2–8 Gyr. However, the presence of these stars cannot give noticeable enhancement of ancient star formation in our model (see Fig. 6). Another, more general problem affecting any population modelling is the ability (or inability) of theoretical isochrones to fully account for all features in an observed CMD (see, e.g., Langer & Maeder 1995 for red and blue supergiants).

We find a dominant episode of star formation with an age range from about 6 to about 200 Myr. The mean star formation rate (SFR) during this period was $7.5^{+2.6}_{-2.2}\cdot 10^{-3}$ $M_\odot$ yr^{-1} with a metallicity spanning $-0.7 \leq$ [Fe/H] ≤ -0.4. The wide range in metallicities can indicate that the method is unable to resolve metallicity differences of $\leq$0.3 dex in our data. For instance, differences in the location of main sequence stars caused by metallicity within this range become indistinguishable in the presence of differential reddening. There are no clear signs of older star formation although, given the limitations of the data, we cannot exclude the presence of sparse older populations.

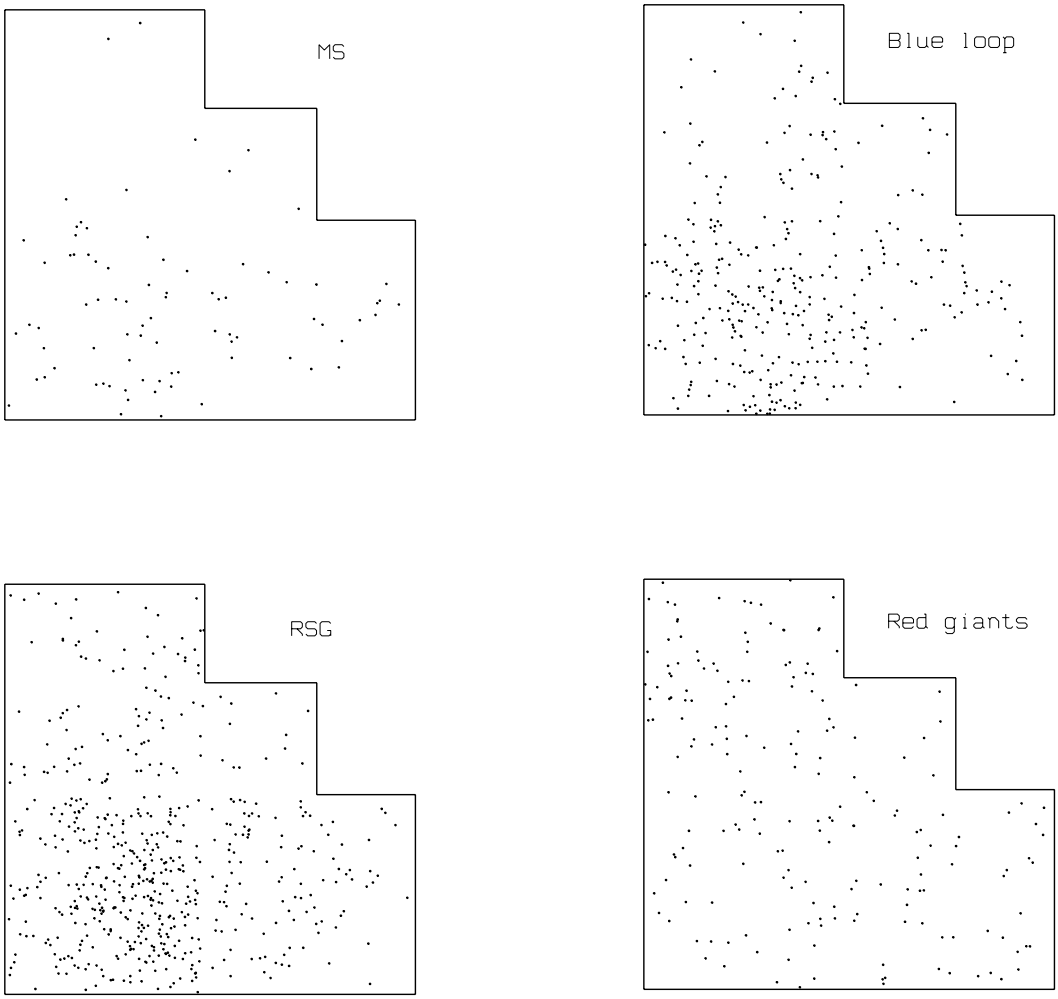

Fig. 5. Spatial distribution of the stellar populations in Holmberg IX. The main sequence stars (their age range is about 10–100 Myr) is bounded by $(V - I)_0 < 0$ and $I_0 \leq 23.75$. The boundaries of the shown blue loop (~10–200 Myr) are: $0 \leq (V - I)_0 \leq 0.75$ and $I_0 \leq 23.75$. RSG stars (~10 Myr–1 Gyr) correspond to the range: $(V - I)_0 > 0.75$ and $I_0 \leq 23.75$. The probable red giants (>1 Gyr) bounded by $(V - I)_0 \geq 0.8$ and $23.75 \leq I_0 \leq 24.5$.

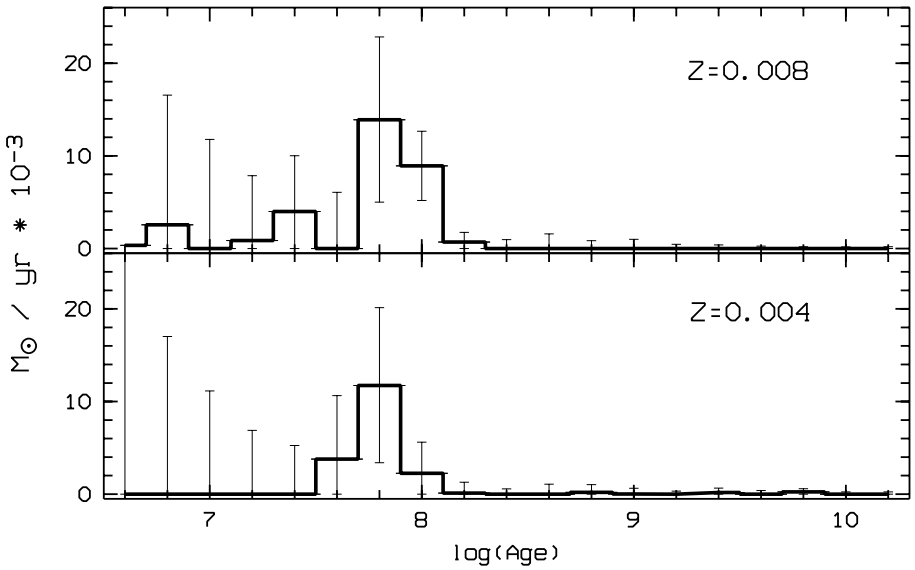

Fig. 6. The best-fit SFH for Holmberg IX. Error bars on the SFH amplitudes are determined by identifying the 68% (1 σ) confidence interval on each amplitude (see Harris & Zaritsky 2001 for details).

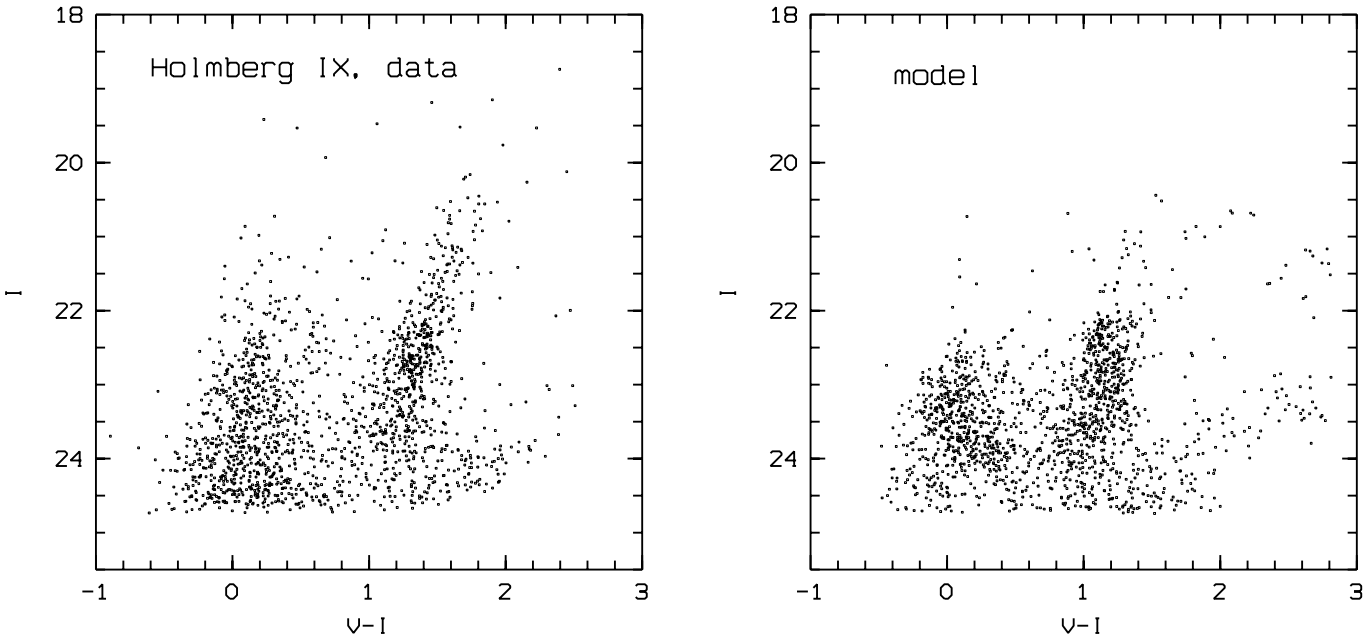

Fig. 7. The best-fit model CMD (right panel) and observed CMD (left panel) of Holmberg IX.

Thus, we can see continuous star formation in Holmberg IX from about 6 until 200 Myr ago and probably also a small number of younger stars. Therefore, Holmberg IX may indeed be a very young tidal dwarf galaxy formed out of tidal debris from the interaction between M 81 and M 82. An indirect confirmation of the age estimation comes from results of a numerical simulation of the dynamical evolutionary history of the M 81–M 82–NGC 3077 system (Yun 1999): The nearest approach between M 82 and M 81 was 220 Myr ago according to this work, which is in good agreement with our result.

Spectroscopic observations of Holmberg IX were carried out at the 6-m BTA telescope (Special Astrophysical Observatory, Russia) by S. A. Pustilnik and A. G. Pramsky using the fast spectrograph of the prime focus (see the equipment description on `http://www.sao.ru/Doc-en//Telescopes/bta/instrum/instrum.html`). The slit was placed on one of H II regions, which was found within the galaxy field by Miller & Hodge (1994) (region number 8). This region is also visible in our WFPC2 field. The spectrum of this object is rather weak, and only Hβ, Hα and weak [NII]λ6584 are seen. Using an empirical relation between O/H and the flux ratio of [NII]λ6584 and Hα (van Zee et al. 1998; Denicoló et al. 2002), the derived 12+log(O/H) value is equal to 8.50 with probable rms uncertainty of 0.15 dex (or [O/H] = −0.42). The latter corresponds to an ionized gas metallicity of $Z \approx 0.0076$. This value falls within the stellar population metallicity range found in our modelling.

4.3. BK3N

This small galaxy is located at the southwestern side of M 81, almost symmetrically to Holmberg IX at the opposite side of M 81 (see Fig. 4). However, in distinction to Holmberg IX, signs of RGB stars in the CMD of BK3N can be recognized. Other than that, mainly blue loop/blue main sequence stars and red supergiants are present in the diagram.

The spatial distribution of resolved stars in the object is shown in Fig. 8. We can see the strong concentration of the upper main sequence stars ($(V-I)_0 \leq 0$) towards the galaxy. The blue loop also exhibits a very clear concentration to BK3N, albeit with a larger spatial extent. The red supergiants show a less concentrated distribution and trace the body of the dwarf only marginally. In the right bottom part of Fig. 8 the distribution of red giants is shown. We can distinguish a marginal increase in the stellar density toward M 81 and absence of any concentration of this population towards BK3N. This seems to indicate that the red giants in the CM diagram of this dwarf galaxy belong to M 81. Like Holmberg IX, this makes BK3N another candidate of a young tidal dwarf galaxy.

The small number of red and blue supergiants in the CMD of BK3N causes very large uncertainties in the SFR determination, and the χ^2 uncertainty for the fitting is 2.3. The result of the SFH computation for this galaxy is presented in Fig. 9. The most significant star formation occurred in this galaxy about 8–200 Myr ago, as can be seen from the histogram in Fig. 9. The star formation rate in this period is estimated to be $3.8^{+8.9}_{-1.7} \times 10^{-4}$ $M_\odot$ yr^{-1} with a metallicity range to be –0.7≤[Fe/H]≤0. The formally allowable metallicity spread is thus even larger than for Holmberg IX. The large uncertainty in the SFH determination does not allow us to draw reliable conclusions about ancient star formation in this galaxy. Nevertheless, some star formation may have taken place about 500 Myr–2 Gyr ago and 8–12 Gyr ago with a probably lower metal abundance ([Fe/H] about –0.7). The original and model CM diagrams are presented in Fig. 10. Like for the previous galaxy, we can see some deficiency of bright red and blue stars in the model CMD, but the main features in the diagram correspond to the observed populations, and red giants, which probably belong to M 81, are also reproduced in our model (see Fig. 10). However, the

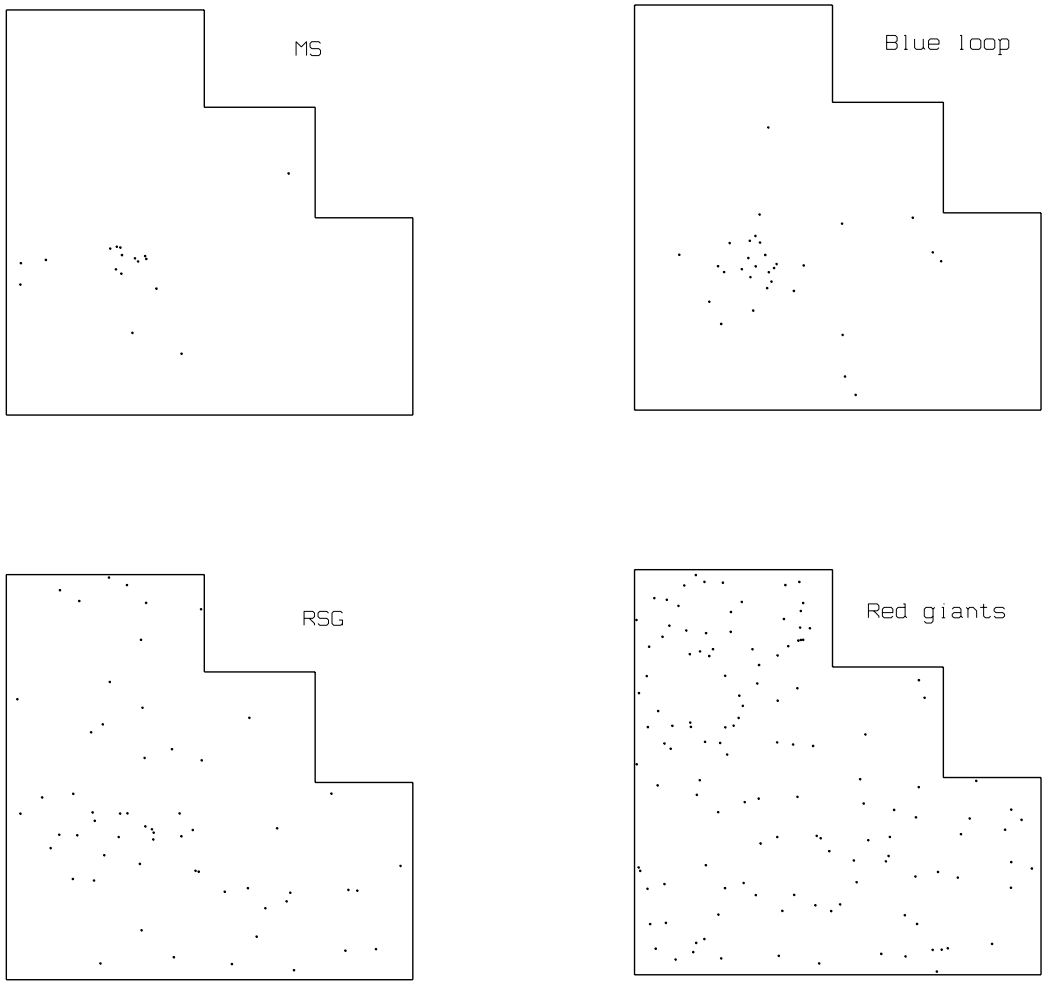

Fig. 8. Spatial distribution of the stellar populations in BK3N. The main sequence stars (∼10–100 Myr) is bounded by $(V-I)_0 < 0$ and $I_0 \leq 24.5$. The boundaries of the blue loop (∼10–100 Myr) are: $0 \leq (V-I)_0 \leq 0.75$ and $I_0 \leq 24.5$. RSG stars (∼10 Myr–1 Gyr) correspond to the range: $(V-I)_0 > 0.75$ and $I_0 \leq 23.75$. The red giants (>1 Gyr) bounded by $(V-I)_0 \geq 0.8$ and $23.75 \leq I_0 \leq 24.5$.

data quality for this object is so poor that modelling will remain ambiguous. Deeper data are clearly needed.

The potential presence of the intermediate-age stars (500 Myr–2 Gyr) in the galaxy may indicate that BK3N formed before the tidal interaction in the core M 81 group. However, these stars may also have been stripped from M 81's outer parts during the interaction.

4.4. Arp-loop (A0952+69)

This object is the brightest part of the diffuse circular structure that embraces the northern part of M 81. Our observations of this galaxy at the 3.5-m telescope of Apache Point Observatory (USA) show that Arp-loop has an extremely low surface brightness, which is fainter than 26 mag arcsec^{-2} in the V band (Makarova et al. 2002).

The color-magnitude diagram of Arp-loop contains the smallest number of stars (about 250) among the four galaxies studied (see Fig. 2).

The spatial density distribution for the resolved stars in the galaxy CMD is shown in Fig. 11. There are only a few objects with $(V-I)_0 \leq 0$, which may belong to the upper MS of Arp-loop, or which could in part be background point sources. The distribution of blue loop stars shows a clear concentration toward the center of the galaxy. These stars trace star formation regions in the galaxy very clearly, as do the RSG stars, which are similarly concentrated. Red giants also smoothly trace the galaxy overall structure and exhibit a clear concentration toward the center of Arp-loop, which supports the idea that they belong to Arp-loop rather than to M 81. However, the location of these stars in the WFPC2 field coincides with the direction toward M 81. It is conceivable that one can see the northern part of M 81's outer edge of red giant disk.

The best-fit SFH for this galaxy is shown in Fig. 12. For this model, the χ^2 value is 1.5. We find a dominant episode within an age interval of about 40–160 Myr ago and a metallicity spanning a range of [Fe/H] = −1.3 dex to −0.4 dex. We obtain the mean star formation rate of $3.6^{+9.7}_{-2.1} \times 10^{-4}$ $M_\odot$ yr^{-1}. A less intensive star formation episode may have taken place about 500 Myr to 1 Gyr ago. One can also see signs of earlier star formation about 5 to 8 Gyr ago with a SFR of $2.2^{+5.2}_{-1.6} \times 10^{-4}$ $M_\odot$ yr^{-1} and a metallicity spanning a range of [Fe/H] = −1.3 to −0.7 dex. The photometric limit does not allows us to detect older stars in this galaxy. The resulting

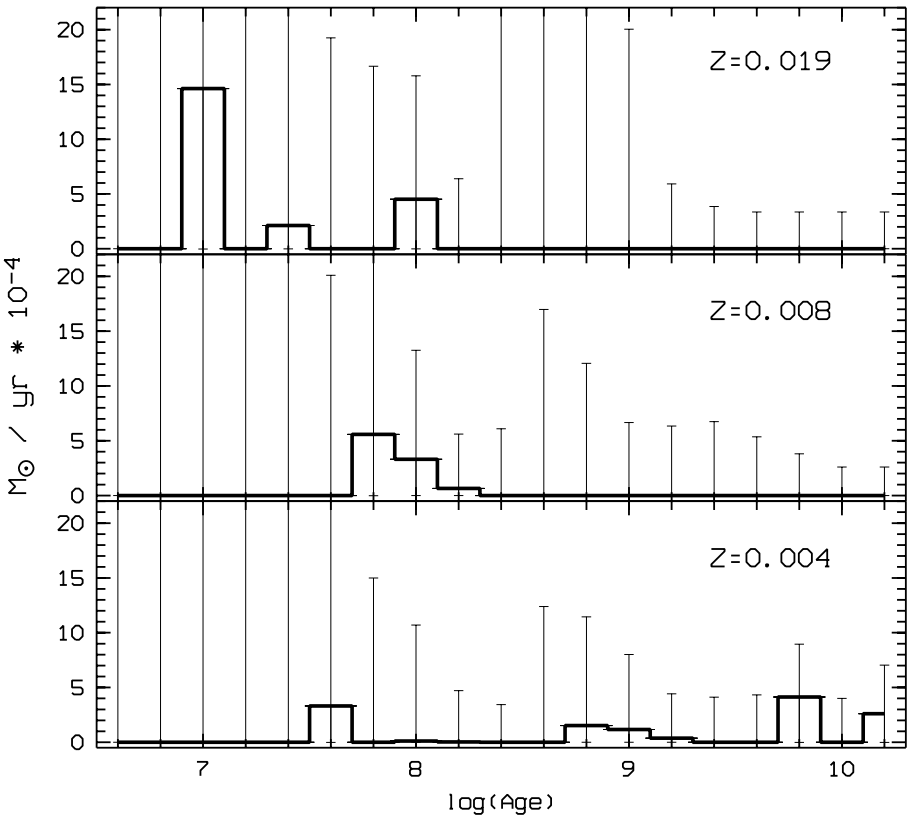

Fig. 9. The best-fit SFH for BK3N.

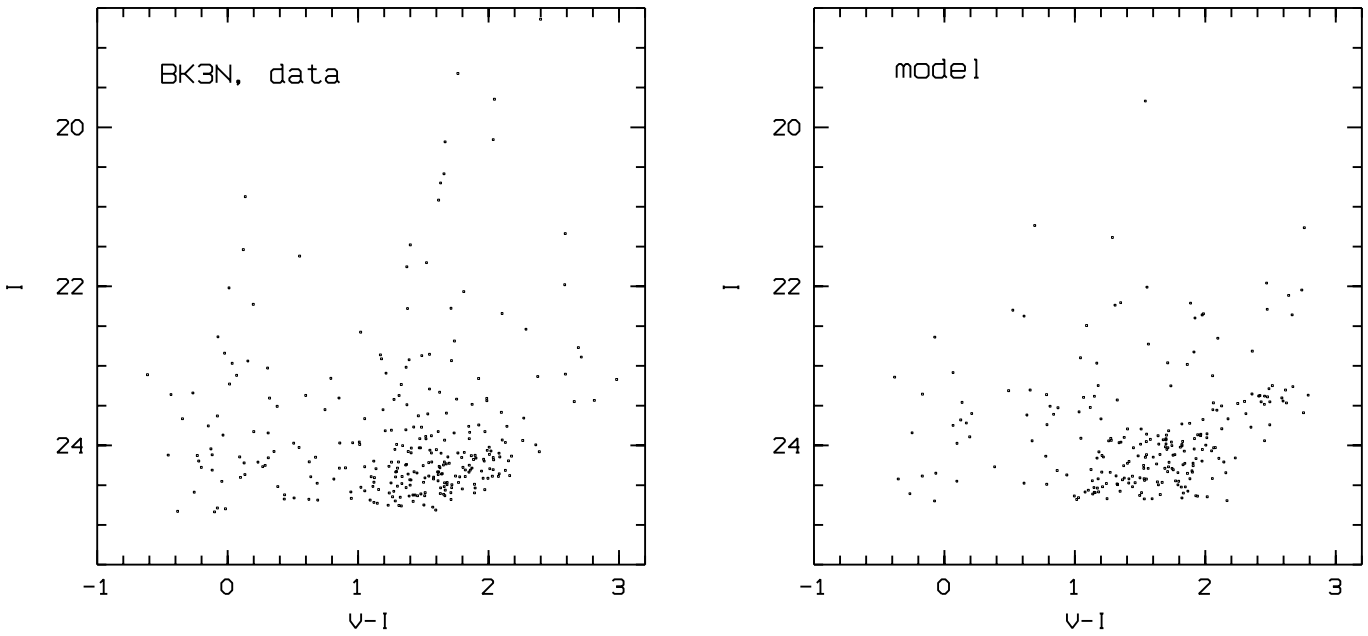

Fig. 10. The best-fit model CMD (right panel) and observed CMD (left panel) of BK3N.

model CM diagram for Arp-loop is shown in the right panel of Fig. 13. As we can see from the comparison with the observational data (left panel in Fig. 13), there is a good agreement of these two diagrams.

Thus one possible conclusion from our data is that Arp-loop may be a pre-existing dIrr galaxy undergoing strong interaction with M 81. On the other hand, red giants in Arp-loop show a clear concentration toward the direction of M 81. They are presumably at least in part constituents of the outer part of M 81's red giant disk. If all of the red giants in fact belong to M 81, then this would make Arp-loop into a tidal dwarf with an age of approximately 1 Gyr. Alternatively, Arp-loop could be part of an outer spiral arm of M 81 with very low surface brightness.

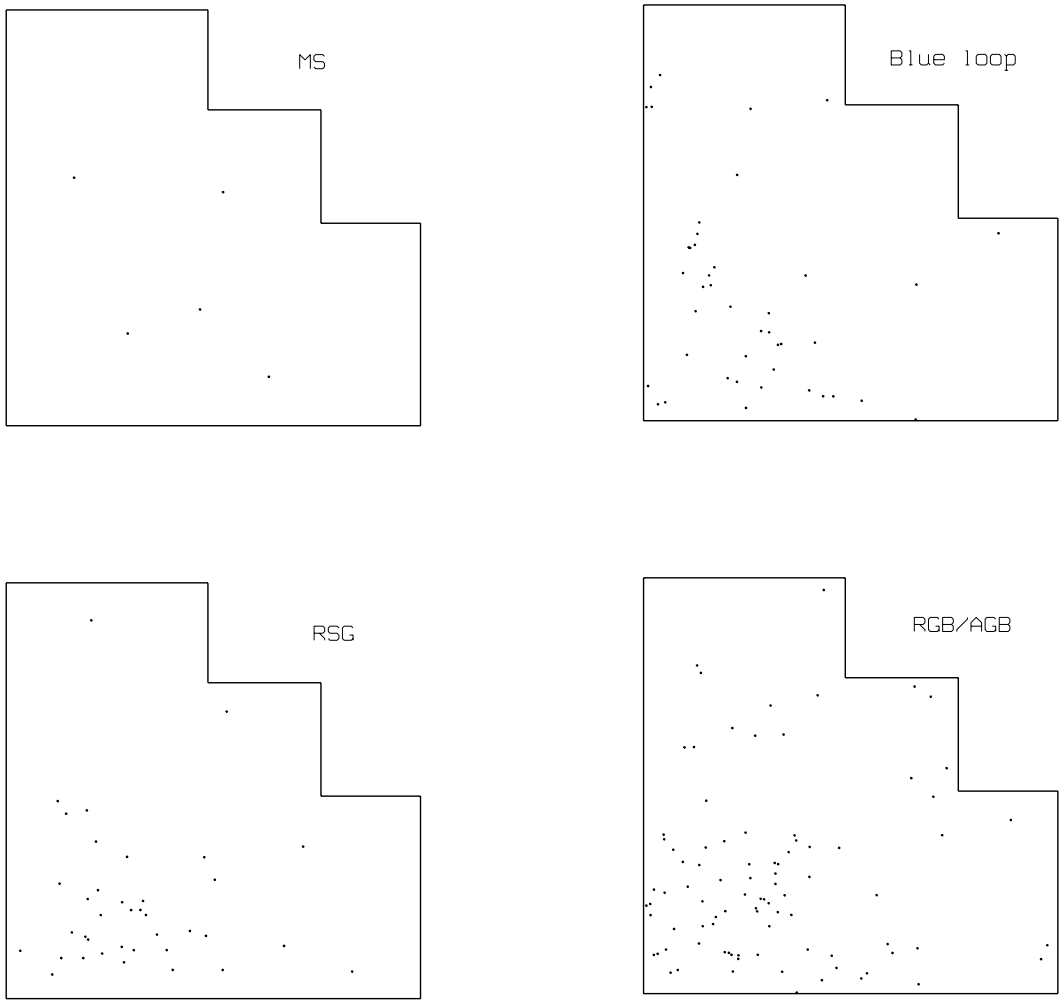

Fig. 11. Spatial distribution of the stellar populations in Arp-loop. The main sequence stars (~40–200 Myr) is bounded by $(V-I)_0 < 0$ and $I_0 \leq 24.5$. The boundaries of the blue loop (~40–200 Myr) are: $0 \leq (V-I)_0 \leq 0.75$ and $I_0 \leq 24.5$. RSG stars (~40 Myr–1 Gyr) correspond to the range: $0.75 < (V-I)_0 \leq 2$ and $I_0 \leq 23.75$. The red giants (>1 Gyr) bounded by $(V-I)_0 \geq 0.8$ and $23.75 \leq I_0 \leq 24.5$.

4.5. Garland

Garland is situated very close to NGC 3077, and all of the WFPC2 field is filled with AGB/RGB stars that appear to belong to NGC 3077. The stellar population of Garland was recently studied in some detail by Sakai & Madore (2001). Their observations were made with HST/WFPC2 using the F555W and F814W filters. The resulting CMDs are $1\overset{m}{.}5$ deeper than ours. The authors obtained a TRGB distance modulus of the galaxy of $\mu_0 = 27.93$ mag. The distance modulus $\mu_0 = 27.89$ mag found by Karachentsev et al. (2002) is in good agreement with the result of Sakai & Madore (2001).

However, neither the data of Sakai and Madore, nor our data allow us to confirm or rule out the presence of RGB stars in Garland itself. Hence it is unclear whether the derived distance refers to NGC 3077, to Garland, or to both. We use theoretical isochrones of $Z = 0.004$ to fit the color-magnitude diagram of Garland, taking into account Sakai & Madore's (2001) estimation of the RGB metallicity ($Z = 0.005$) from the colors of the RGB stars. The isochrones fit the CMD quite well, except for some red stars with $(V-I)_0 > 2$ and $I_0 < 21$, which may be Galactic foreground stars.

The spatial distribution of the resolved stellar population is shown in Fig. 14. It clearly demonstrates the large number of NGC 3077 RGB stars. There is also a population of upper main sequence stars with $(V-I)_0 \leq 0$ and $I_0 > 22$ which trace an arc-like structure distinct from the distribution of the RGB stars.

Unfortunately, the algorithm used for the SFH calculation did not result in an acceptable fit. Therefore, we decided to omit a quantitative SFH analysis here. In general, we can recognize in the CMD evidence for star formation in age intervals similar to the two previous galaxies. Namely, recent episode of star formation probably occurred about 16–200 Myr ago.

As noted by Sakai & Madore, for the case of Garland, it is conceivable that recent star formation (16–200 Myr ago) was triggered as a direct result of the tidal interaction of the galaxy in the core M 81 group. However, the overall age and nature of this feature near NGC 3077 remain uncertain due to the presence of a large number of NGC 3077 red giant stars in the Garland field.

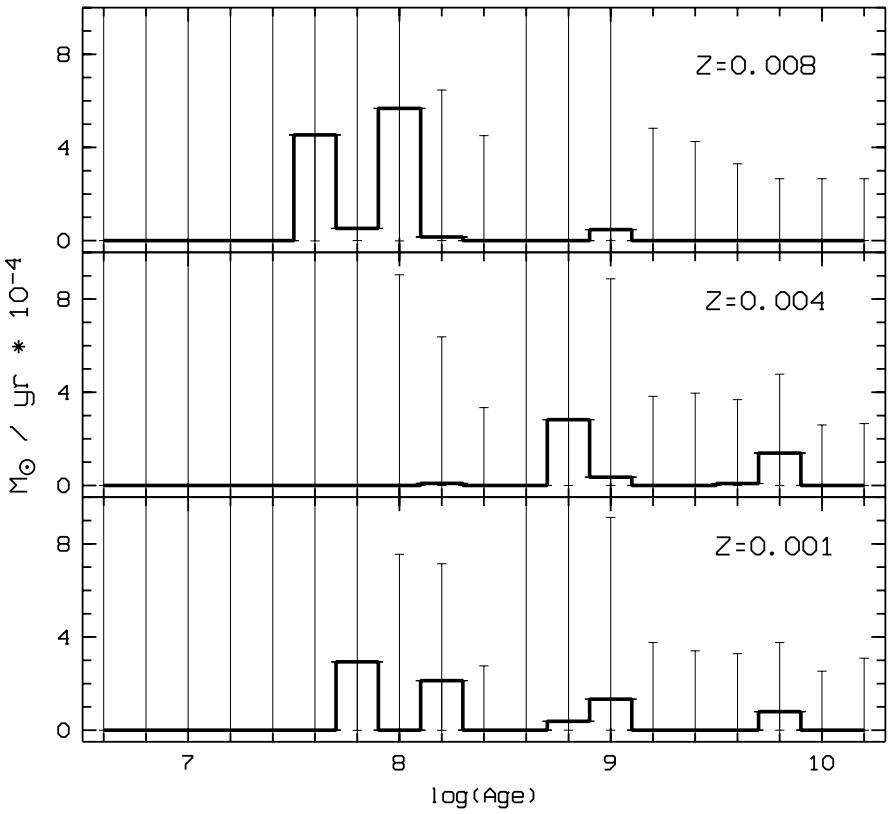

Fig. 12. The best-fit SFH for Arp-loop.

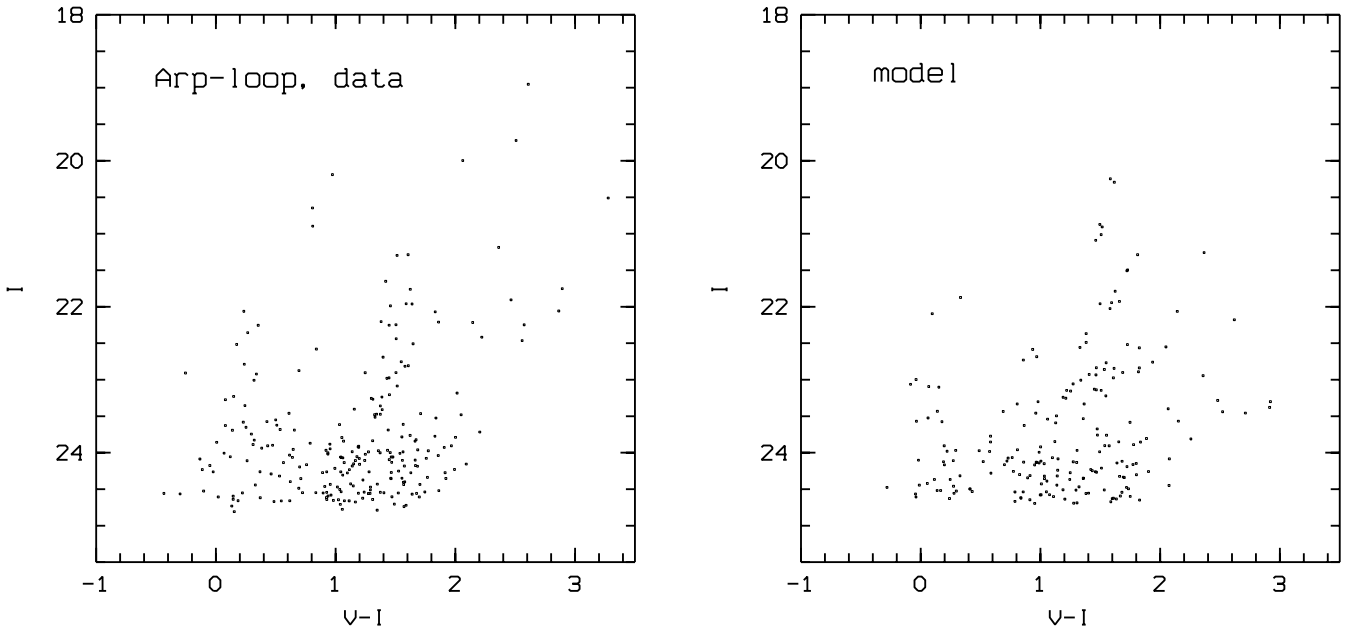

Fig. 13. The best-fit model CMD (right panel) and observed CMD (left panel) of Arp-loop.

5. Discussion and conclusion

We investigated the question of whether the four dIrr galaxies Holmberg IX, BK3N, Arp-loop, and Garland, whose projected positions coincide with density peaks in the H I tidal streams in the interacting M 81 group, could be tidal dwarf galaxies.

Table 2 summarizes the results of the synthetic CMD modelling of our HST/WFPC2 data for the suspected tidal dwarfs. The distances to the galaxies and Galactic foreground extinction values used in the computation are given in Cols. 2–4 of Table 2.

The photometric limits of our images do not allow us to clarify the evolutionary status of the four dwarf irregular galaxies with good accuracy. However, a comparison of the star formation ages in the galaxies derived via synthetic CMD

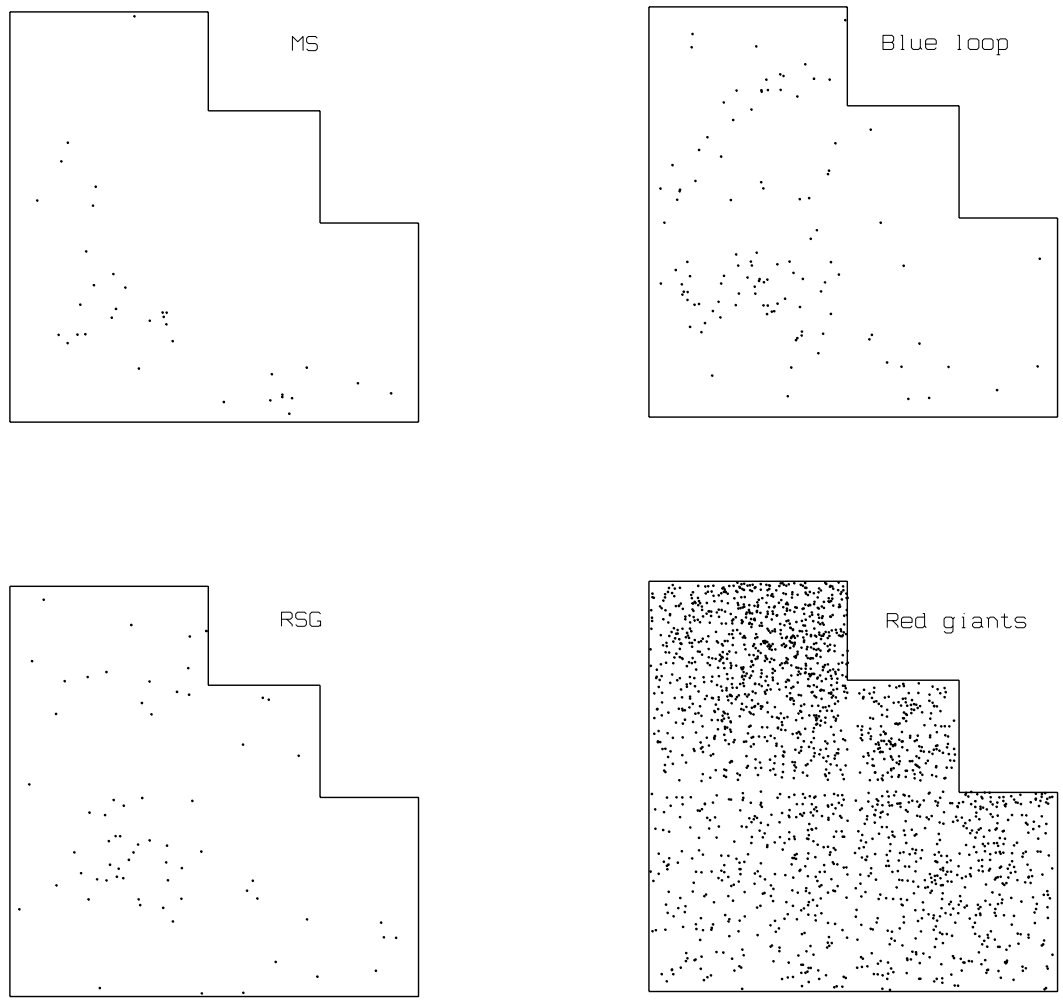

Fig. 14. Spatial distribution of the stellar populations in Garland. The main sequence stars (~20–160 Myr) is bounded by $(V-I)_0 < 0$ and $I_0 \leq 24.5$. The boundaries of the blue loop (~20–160 Myr) are: $0 \leq (V-I)_0 \leq 0.75$ and $I_0 \leq 24.5$. RSG stars (~20–160 Myr) correspond to the range: $0.75 < (V-I)_0 \leq 2$, $I_0 \leq 23.75$ and $(V-I)_0 > 2$, $I_0 \geq 22$. The red giants (>1 Gyr) bounded by $(V-I)_0 \geq 1$ and $23.75 \leq I_0 \leq 24.5$.

Table 2. Star formation history of the tidal dwarfs.

Name	$E(V-I)$ [mag]	A_I [mag]	μ_0 [mag]	Star formation age	mean SFR [$M_\odot$ yr^{-1}]	[Fe/H] [dex]
Holmberg IX	0.109	0.154	27.80	6–200 Myr	$7.5^{+2.6}_{-2.2} \times 10^{-3}$	–0.7 ÷ –0.4
BK3N	0.110	0.155	27.80	8–200 Myr	$3.8^{+8.9}_{-1.7} \times 10^{-4}$	–0.7 ÷ 0.0
				500 Myr–2 Gyr	$0.8^{+13.4}_{-0.5} \times 10^{-4}$	–0.7
				8–12 Gyr	$2.0^{+2.9}_{-1.4} \times 10^{-4}$	–0.7
Arp-loop	0.117	0.164	27.80	40 Myr–160 Myr	$3.6^{+9.7}_{-2.1} \times 10^{-4}$	–1.3 ÷ –0.4
				500 Myr–1 Gyr	$2.6^{+13.9}_{-1.4} \times 10^{-4}$	–1.3 ÷ –0.4
				5–8 Gyr	$2.2^{+5.2}_{-1.6} \times 10^{-4}$	–1.3 ÷ –0.7
Garland	0.092	0.130	27.89	16–200 Myr :		–0.7 ÷ 0.0
				600 Myr–1 Gyr :		–0.7 ÷ 0.0
				8–10 Gyr :		–0.7 ÷ 0.0

modelling helps us to make some suggestions. As can be seen from Table 2, Holmberg IX, BK3N, and Arp-loop (and probably Garland as well) experienced an episode of enhanced star formation between roughly 20 and 200 Myr ago. The star formation process may have been activated by the tidal interaction between M 81, M 82, and NGC 3077, which is believed to have occurred 220 Myr ago (M 81–M 82) and 280 Myr ago (M 81–NGC 3077) according to numerical simulations by Yun (1999).

There are also intermediate age stars in Arp-loop and BK3N (and probably in Garland, too). These stars may

indicate that these two (three) galaxies existed already prior to the tidal interaction, or contain older stellar material torn out of the massive galaxies during the interaction. Finally, some star formation may have occurred in Arp-loop and BK3N ≥ 8 Gyr ago, but these older stars have magnitudes close to our detection limit, which makes their interpretation difficult. While the young populations show a clear spatial coincidence and concentration toward the centers of the dwarf galaxies, this is less pronounced for the older populations. The proposed old red giant branch population may in fact belong to the extended old population of M 81 (and NGC 3077) and could be seen in projection along the line of sight to the dwarfs. In the case of Holmberg IX no significant indications of star formation longer ago than ~200 Myr ago could be detected.

Judging from the results of the synthetic CMD modelling, the metallicity of the detected stars shows a spread of up to 1 dex and is relatively high (up to −0.4 dex in [Fe/H]). While the caveats of deriving photometric metallicities of young populations via isochrones should be kept in mind, these relatively high values (for low-mass dwarf galaxies) may support a tidal origin, although they remain below the abundances measured in M 81 H II regions.

Considering the similarity of the star formation histories of the four dwarfs, they may all have formed from material of the metal-poor outer part of the giant spiral galaxy M 81 after the tidal interaction event about 200 Myr ago. The ultimate confirmation of this scenario will require significantly deeper CMDs than our present HST data provide.

Acknowledgements. We are very grateful to S. A. Pustilnik and A. G. Pramsky for kindly making available to us the results of their spectroscopic measurements. LNM thanks J. Harris for his help with the program package starFISH. The work of LNM was supported by INTAS grant YSF 2001/1-0129 and by the Max-Planck Institute for Astronomy, Heidelberg. LNM, IDK and MES acknowledge support through the Russian Foundation for Base Research Grant 01-16001. D.G. gratefully acknowledges support from the Chilean *Centro de Astrofísica* FONDAP No. 15010003.

References

Appleton, P., Davies, R., & Stephenson, R. 1981, MNRAS, 195, 327
Bahcall, J. N., & Soneira, R. M. 1981, ApJS, 47, 357
Bertelli, G., Bressan, A., Chiosi, C., Fagotto, F., & Nasi, E. 1994, A&AS, 106, 275
Boerngen, F., & Karachentseva, V. E. 1982, AN, 303, 189
Boyce, P. J., Minchin, R. F., Kilborn, V. A., et al. 2001, ApJ, 560, L127
Denicoló, G., Terlevich, R., & Terlevich, E. 2002, MNRAS, 330, 69
Dolphin, A. E. 2000a, PASP, 112, 1383
Dolphin, A. E. 2000b, PASP, 112, 1397
Dolphin, A. E., Makarova, L., Karachentsev, I. D., et al. 2001, MNRAS, 324, 249
Freedman, W. L., Hughes, Sh. M., Madore, B. F., et al. 1994, ApJ, 427, 628
Gardiner, L. T., Sawa, T., & Fujimoto, M. 1994, MNRAS, 266, 567
Girardi, L., Bressan, A., Bertelli, G., & Chiosi, C. 2000, A&AS, 141, 371
Grebel, E. K., Seitzer, P., Dolphin, A. E., et al. 2000, in Stars, Gas, and Dust in Galaxies: Exploring the Links, ed. D. Alloin, K. Olsen, & G. Galaz (San Francisco: ASP), ASP Conf. Ser., 221, 147
Harbeck, D., Grebel, E. K., Holtzman, J., et al. 2001, AJ, 122, 3092
Harris, J., & Zaritsky, D. 2001, ApJS, 136, 25
Heithausen, A., & Walter, F. 2000, A&A, 361, 500
Hughes, S. M. G., Stetson, P. B., Turner, A., et al. 1994, ApJ, 428, 143
Hunter, D. A., Hunsberger, S. D., & Roye, E. W. 2000, ApJ, 542, 137
Ibata, R. A., Gilmore, G., & Irwin, M. J. 1994, Nature, 370, 194
Karachentseva, V. E., Karachentsev, I. D., & Boerngen, F. 1985, A&AS, 60, 213
Karachentsev, I. D., Karachentseva, V. E., & Huchtmeier, W. K. 2001, A&A, 366, 428
Karachentsev, I. D., Sharina, M. E., Grebel, E. K., et al. 1999, A&A, 352, 399
Karachentsev, I. D., Karachentseva, V. E., Dolphin, A. E., et al. 2000, A&A, 363, 117
Karachentsev, I. D., Sharina, M. E., Dolphin, A. E., et al. 2001, A&A, 375, 359
Karachentsev, I. D., Dolphin, A. E., Geisler, D., et al. 2002, A&A, 383, 125
Langer, N., & Maeder, A. 1995, A&A, 295, 685
Lee, M., Freedman, W., & Madore, B. 1993, ApJ, 417, 553
Makarova, L. N., Karachentsev, I. D., Grebel, E. K., & Barsunova, O. Yu. 2002, A&A, 384, 72
Miller, B. W., & Hodge, P. 1994, ApJ, 427, 656
Sakai, Sh., & Madore, B. 2001, ApJ, 555, 280
Seitzer, P., Grebel, E. K., Dolphin, A. E., et al. 1999, AAS, 195, 801
Schlegel, D. J., Finkbeiner, D. P., & Davis, M. 1998, ApJ, 500, 525
van der Hulst, J. M. 1977, Ph.D. Thesis, Univ. Groningen
van Driel, W., Kraan-Korteweg, R., Binggeli, B., & Huchtmeier, W. 1998, A&AS, 127, 397
van Zee, L., Salzer, J. J., Haynes, M. P., O'Donoghue, A. A., & Balonek, T. J. 1998, AJ, 116, 2805
Yun, M., Ho, P., & Lo, K. 1994, Nature, 372, 530
Yun, M. S. 1999, IAU Symp., 186, 81